Human Molecular Genetics, 2016, Vol. 25, No. 14 3042–3054

doi: 10.1093/hmg/ddw157
Advance Access Publication Date: 6 June 2016
Original Article

ORIGINAL ARTICLE

Neuronal deficiency of *ARV1* causes an autosomal recessive epileptic encephalopathy

Elizabeth E. Palmer[1,2,†], Kelsey E. Jarrett[3,4,†], Rani K. Sachdev[1,5], Fatema Al Zahrani[6], Mais Omar Hashem[6], Niema Ibrahim[6], Hugo Sampaio[1,5], Tejaswi Kandula[1,5], Rebecca Macintosh[5], Rajat Gupta[3], Donna M. Conlon[7], Jeffrey T. Billheimer[7], Daniel J. Rader[7], Kouichi Funato[8], Christopher J. Walkey[9], Chang Seok Lee[3], Christine Loo[1,10], Susan Brammah[11], George Elakis[10], Ying Zhu[2,10], Michael Buckley[10], Edwin P. Kirk[1,5,10], Ann Bye[1,5], Fowzan S. Alkuraya[6], Tony Roscioli[5,12,13,‡] and William R. Lagor[3,*,‡]

[1]Department of Women and Children's Health, Randwick Campus, University of New South Wales, NSW 2031, Australia, [2]Genetics of Learning Disability Service, Waratah, NSW 2298, Australia, [3]Department of Molecular Physiology and Biophysics, [4]Integrative Molecular and Biomedical Sciences Graduate Program, Baylor College of Medicine, Houston, TX 77030, USA, [5]Sydney Children's Hospital, Randwick, NSW 2031, Australia, [6]Department of Genetics, King Faisal Specialist Hospital and Research Center, Riyadh 11211, Saudi Arabia, [7]Division of Translational Medicine and Human Genetics, Perelman School of Medicine, University of Pennsylvania, Philadelphia, PA 19104, USA, [8]Department of Biofunctional Science and Technology, Graduate School of Biosphere Science, Hiroshima University, 1-4-4 Kagamiyam, Higashi-Hiroshima 739-8528, Japan, [9]Department of Molecular and Cellular Biology, Baylor College of Medicine, Houston, TX 77030, USA, [10]SEALS pathology, Randwick, NSW 2031, Australia, [11]Electron Microscope Unit, Concord Repatriation General Hospital, Concord, NSW 2139, Australia, [12]Kinghorn Centre for Clinical Genomics, Garvan Institute, 370 Victoria St Darlinghurst, Sydney, Australia and [13]St Vincent's Clinical School, University of New South Wales, Sydney, Australia

*To whom correspondence should be addressed at: Molecular Physiology and Biophysics, Baylor College of Medicine Mail Stop BCM335, One Baylor Plaza, Houston TX 77030, USA. Tel: +713.798.8666; Fax +713-798-3475; Email: lagor@bcm.edu

Abstract

We report an individual who presented with severe neurodevelopmental delay and an intractable infantile-onset seizure disorder. Exome sequencing identified a homozygous single nucleotide change that abolishes a splice donor site in the *ARV1*

[†]The authors wish it to be known that, in their opinion, the first two authors, should be regarded as joint First Authors, and the last two authors[‡] as joint Senior Authors.

The accession number for the novel variant reported in this article is ClinVar SCV000262756.

Received: March 14, 2016. **Revised:** April 29, 2016. **Accepted:** May 18, 2016

gene (c.294 + 1G > A homozygous). This variant completely prevented splicing in minigene assays, and resulted in exon skipping and an in-frame deletion of 40 amino acids in primary human fibroblasts (NP_073623.1: p.(Lys59_Asn98del). The p.(Lys59_Asn98del) and previously reported p.(Gly189Arg) *ARV1* variants were evaluated for protein expression and function. The p.(Gly189Arg) variant partially rescued the temperature-dependent growth defect in *arv1*Δ yeast, while p.(Lys59-Asn98del) completely failed to rescue at restrictive temperature. In contrast to wild type human *ARV1*, neither variant expressed detectable levels of protein in mammalian cells. Mice with a neuronal deletion of *Arv1* recapitulated the human phenotype, exhibiting seizures and a severe survival defect in adulthood. Our data support *ARV1* deficiency as a cause of autosomal recessive epileptic encephalopathy.

Introduction

ARV1 (ACAT related enzyme 2 required for viability 1: MIM *611647), located at 1q42.2, encodes a 271 amino acid protein of unknown function. ARV1 is a transmembrane protein of the endoplasmic reticulum (ER) that contains a cytosolic N-terminal zinc binding motif, followed by several transmembrane domains, with the extreme C-terminus of the protein facing the ER lumen. Deletion of *ARV1* in yeast results in multiple growth and viability defects (1–5), abnormal sterol trafficking (1), reduced sphingolipid (2), and glycosylphosphatidylinositol (GPI) anchor synthesis, ER stress (6–8), membrane disorganization (9), and hypersensitivity to fatty acids (5). *ARV1* is conserved across eukaryotic species and ubiquitously expressed at a low level in all tissues (1,10). We recently found that germline deletion of *Arv1* in mice results in a lean phenotype with increased energy expenditure and improved glucose tolerance, identifying *Arv1* as an important component in mammalian energy homeostasis (10). Expression of human *ARV1* can rescue many growth and viability defects in yeast lacking this gene (1–3,7,11). This functional conservation implies an important role for ARV1 in lipid/membrane homeostasis, but until now direct evidence of its role in human disease has been lacking.

We recently reported a homozygous missense variant (NM_022786.1: c.565G > :NP_073623.1p.(Gly189Arg)) in *ARV1* in a male born to consanguineous Saudi parents with severe intellectual disability, early onset epileptic encephalopathy, poor head control and ataxia (12). The proband's brother died, aged 4, of a similar neurodevelopmental disorder; he was strongly suspected to have the same genetic condition but DNA was unavailable for testing. Further segregation studies in this extended family were supportive of pathogenicity: two second cousins (a male and a female), with overlapping phenotype of epileptic encephalopathy, profound intellectual disability, ataxia and visual impairment, were homozygous for the same variant. The underlying pathophysiology was uncertain as the molecular function of ARV1 was poorly understood.

Here we describe a female individual homozygous for a different *ARV1* variant that abolishes a splice site and leads to an in-frame deletion of 40 amino acids (p.(Lys59_Asn98del)). This in-frame deletion truncates the zinc-binding motif and removes over half of the Arv1 homology domain (AHD), an N-terminal portion of the protein that is required for function in yeast (1,3,4,11). This individual had a severe neurodegenerative course, with an infantile onset epileptic encephalopathy, central hypotonia, peripheral hypertonia, dystonia and congenital visual impairment, and died at 12 months of age. We provide detailed phenotypic information for this individual, comparison with the phenotype of the first family, and supporting genetic evidence. We present molecular studies to confirm the pathogenicity of both *ARV1* variants in yeast and mammalian cells. Lastly, we report that mice with a tissue specific deletion of *Arv1* in the central nervous system also exhibit seizures and spontaneous death. We propose that *ARV1*-deficiency should be considered a bona fide syndrome of developmental delay/intellectual disability with seizures that follows a recessive mode of inheritance.

Results

Clinical presentation

We report an individual with a novel homozygous mutation in *ARV1*. The female proband was delivered at term following an uncomplicated pregnancy. Fetal movements were vigorous. Apgar scores were 9 at 1 and 5 min, and birth parameters were in the normal range (25–75th centile). By 6 weeks of life she was persistently irritable with roving eye movements and demonstrated visual inattention, central hypotonia, peripheral hypertonia, extensor posturing, and dystonia. A minimal pupillary response to light led to a diagnosis of retinal dystrophy consistent with Leber congenital amaurosis (13,14), confirmed by persistently abnormal electrophysiological studies (Supplementary Material, Figure S1). Hypermetropia was present (6.5 diopters bilaterally). Fundal examination showed mild retinal arteriolar attenuation and retinal pigment speckling in the mid-periphery (retinographs not available).

The patient presented in status epilepticus at 4 months of age and subsequently had an intractable seizure disorder characterized by clusters of treatment-resistant multifocal seizures. The EEG profile evolved from normal (6 weeks of age) to a slow background with focal epileptiform activity (4 months) to multifocal epileptiform activity with a slow very disorganized background at 7 months (Fig. 1A and B) to modified hypsarrythmia (9 months). She did not obtain developmental milestones and gradually lost volitional activity and interaction with the external environment. She required enteral tube feeding due to gastroesophageal reflux, poor suck, and oromotor control. Growth was appropriate for age with adequate caloric intake (Supplementary Material, Figure S2). The proband died in hospital at 12 months of age, with intractable seizures and recurrent respiratory infections secondary to aspiration

Metabolic diseases were considered, and quadriceps muscle histology (7 months of age) was abnormal with a relative increase in the proportion of type 1 to type 2 fibers and relatively smaller type 2 fibers (Supplementary Material, Figure S3A and B). Respiratory chain enzymology was normal. Electron microscopy (Supplementary Material, Figure S3C–E) demonstrated a mild variation in muscle fiber size. Redundant basal lamina was seen extending from a single atrophic fiber. Occasional fibers showed short segments of reduplicated basal lamina. Prominent lipid droplets were observed in close contact with clumped mitochondria in a rare fiber. Neonatal brain MRI demonstrated a subtle simplification of sulcation in both frontal lobes, although myelination appeared normal for age. At 7 months of age she was noted to have cerebral central tegmental tract hyperintense signal (CTTH) on T2-weighted MRI with restricted diffusion. This

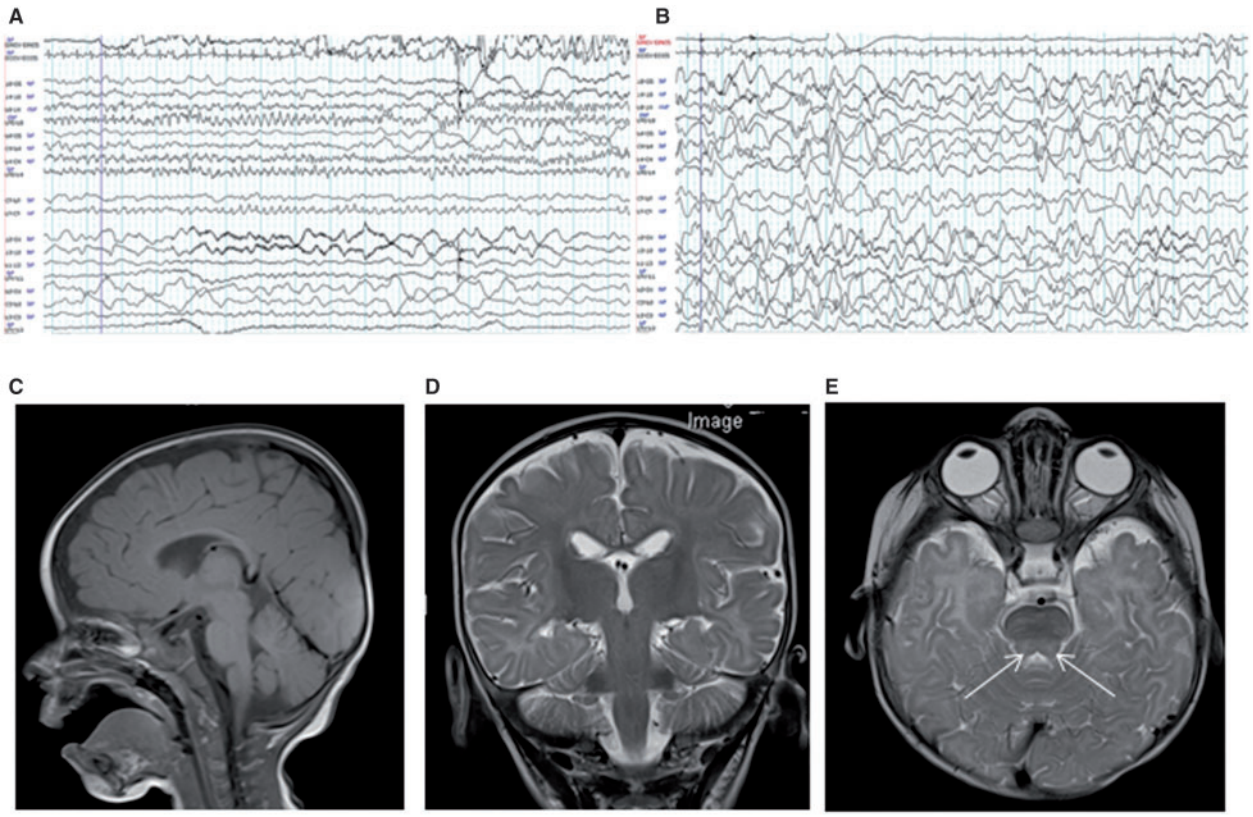

Figure 1. Clinical presentation of proband. Representative electroencephalograms. Longitudinal bipolar EEG montages demonstrating **(A)** evolving focal seizure with build-up of rhythmic activity in the right frontal leads (7 months age); **(B)** modified hypsarrhythmia with high amplitude, poorly organized delta activity and multifocal, posterior dominant spikes at 9 months of age. MRI Brain Images. **(C)** Normal sagittal T1 midline at 5 months and **(D)** coronal T2 image at 7 months. **(E)** Axial T2 weighted images of the patient at 7 months demonstrating symmetric foci of T2 weighted hyperintensity (arrows) within the grey matter nuclei in the posterior pons adjacent to the fourth ventricle. Abbreviations: EEG, electroencephalogram; MRI, magnetic resonance imaging. CSF, cerebrospinal fluid.

was persistent and more prominent at 8 months of age. Representative brain MRI images are shown (Fig. 1C–E).

Family history, exome sequencing, homozygosity mapping, and sanger confirmation

The proband (IV:4 Fig. 2) was the third daughter to consanguineous Lebanese parents. Family history revealed the maternal grandmother had two male infants who died in the newborn period and two miscarriages of unknown cause. Exome sequencing was performed; after filtering there were no obvious candidate variants on heterozygous or *de novo* inheritance models. One homozygous variant stood out as potentially causative of the patient's neurocognitive phenotype (other rare homozygous variants of uncertain significance that were heterozygous in both parents listed in Supplementary Material, Table S1). This was a homozygous variant in *ARV1* that was predicted to result in aberrant splicing (NM_022786.1:c.294 + 1G > A) and to be pathogenic (scaled CADD score v1.3 25.8), affecting an evolutionarily conserved nucleotide (PhyloP score 5.749). It also lay within the largest region of unique homozygosity for the proband on chromosome 1 (Fig. 2B). The variant was listed twice in ExAC v.3 in heterozygous form only (MAF 1.653×10^{-5}). Bidirectional Sanger sequencing confirmed that the proband was homozygous for the variant, each parent was heterozygous, and her siblings were either heterozygous or did not carry the variant (Fig. 2C–E).

The candidacy of *ARV1* was also supported by a different homozygous missense variant, p.(Gly189Arg) in a family with similar phenotypic features of severe-profound intellectual disability and intractable infantile onset epileptic encephalopathy, which we previously reported in a Saudi cohort (12). A more detailed comparison of the phenotype in the two families is provided in Supplementary Material, Table S2. Additional overlapping phenotypic features included movement disorder, visual impairment and premature death. A movement disorder was reported in three individuals: dystonia in the current proband (c. 294 + 1G > A), and ataxia in two patients with the previously reported p.(Gly189Arg) variant. The current proband had a retinal dystrophy. Visual impairment was only reported in one of the three tested individuals with the p.(Gly189Arg) variant, but formal ophthalmological examinations were unavailable so milder visual impairment could not be excluded. The current proband died prematurely at 12 months, the affected sibling of the proband with the p.(Gly189Arg) variant died at 4 years of age.

Analysis of effects of c.294 + 1G > A on splicing

We next sought to determine if the c.294 + 1G > A variant interferes with normal splicing of *ARV1*. To test this, we generated minigene vectors containing *ARV1* exons 2 and 3 surrounding a synthetic intron composed of the first and last 100 bases of intron 2 (Fig. 3). Minigene vectors for the wild type (WT) or c.294 + 1G > A sequence were transfected into HEK293T cells,

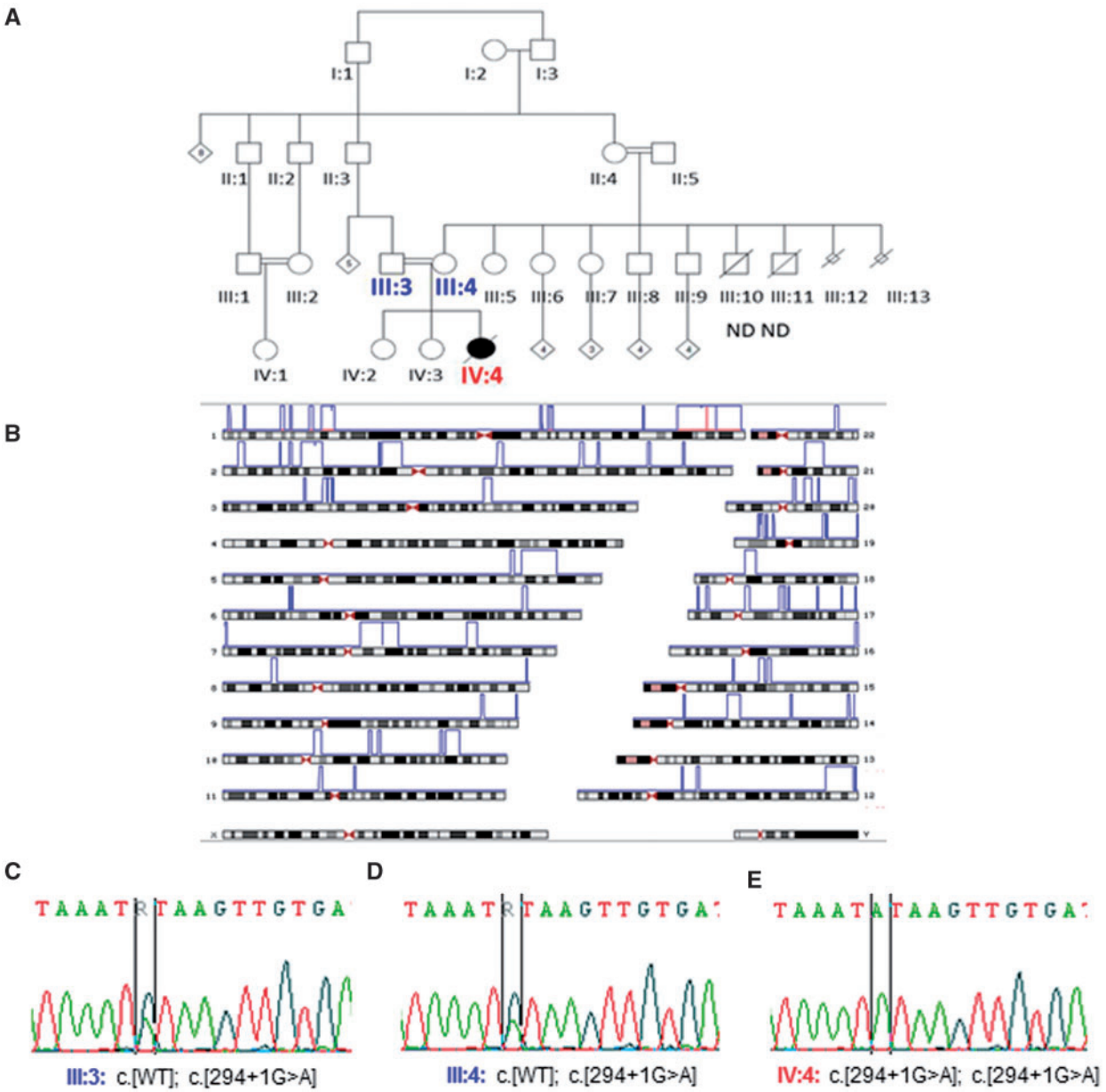

Figure 2. Pedigree, homozygosity mapping, and Sanger sequencing. **(A)** Pedigree for the proband's family. The proband is IV:4. **(B)** Homozygosity mapping for the proband. Parental homozygous regions are subtracted from the Proband (blue); candidate gene *ARV1* shown in red on Chromosome 1. **(C and D)** Each parent (III:3 and III:4) is heterozygous for the splice variant. **(E)** The proband IV:4 is homozygous for splice site variant ARV1_NM_022786: c.294 + 1G > A. The unaffected siblings are either heterozygous or homozygous for reference allele- results not shown for confidentiality. Abbreviations: WT, wild type; ND, neonatal death.

and RNA was isolated and analyzed by RT-PCR. Successful splicing should result in amplification of a 380 bp product, while the unspliced PCR product is 580 bp. In the absence of reverse transcription we observed a 580 bp band derived from plasmid DNA (Fig. 3B) that was fully eliminated by pretreatment with DNAse I (Fig. 3B). Amplification from the DNAse-treated, reverse transcribed cDNA from both WT and c.294 + 1G > A showed unspliced transcript at 580 bp, but only the WT transcript could be efficiently spliced to the correct 380 bp fragment (Fig. 3B).

Sequencing of the c.294 + 1G > A transcript

Since the c.294 + 1G > A variant pre-mRNA was unable to be properly spliced between exons 1 and 2, we sought to further characterize the endogenous *ARV1* transcript. Primary fibroblasts were obtained from the proband and used to isolate total RNA. RT-PCR was performed with primers in exons 1 and 4 to amplify the region of interest from the *ARV1* message. Control fibroblasts produced a PCR product at the expected 322 bp size, while this was completely absent in the proband's fibroblasts. Instead, a truncated 202 bp PCR product was present in the sample from the proband (Fig. 3C). This smaller band resulted from skipping of exon 2, and is predicted to encode an in frame deletion of 40 amino acids [NM_022786.1:r.175_294del:p.(Lys59_Asn98del)] (Fig. 3D). The 40 missing amino acids encode the second half of the AHD, including the last cysteine of the zinc-binding motif (1). Expression of the AHD is both necessary (11) and sufficient (4) to prevent hypersensitivity to sterol binding antibiotics in *arv1Δ*

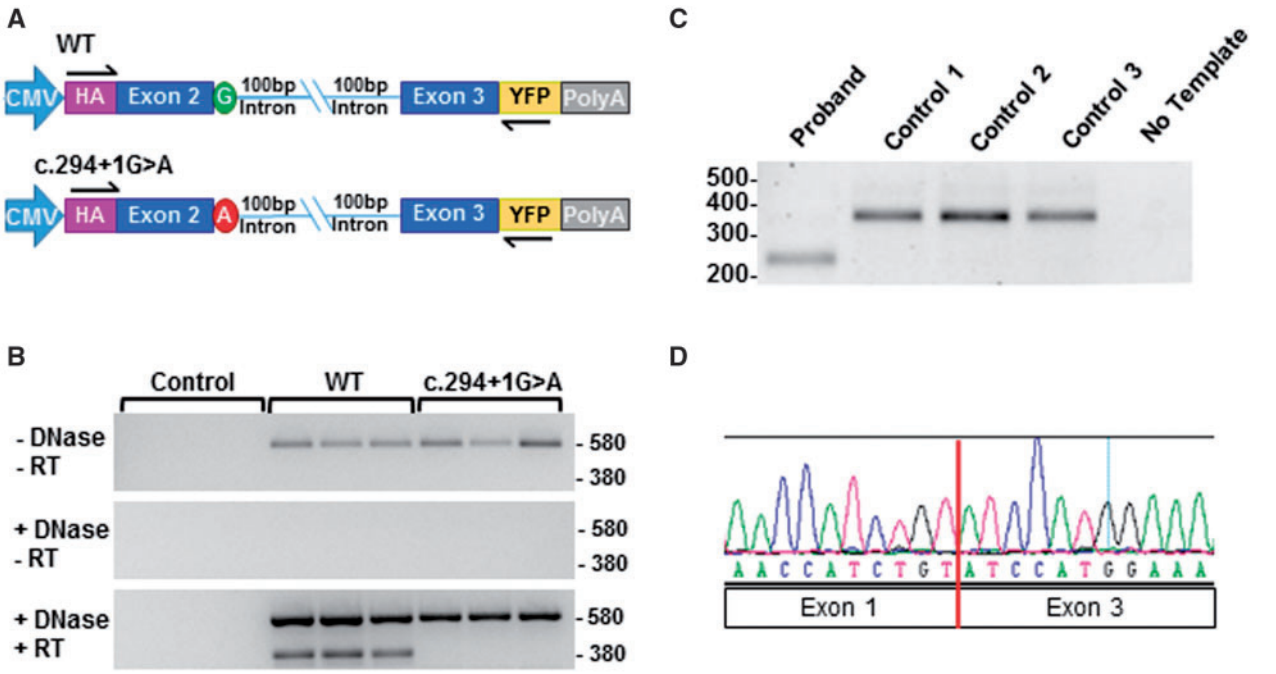

Figure 3. Impact of the *ARV1* c.294 + 1G > A variant on splicing. **(A)** Schematic of minigene constructs used for splicing assay. The c.294 + 1G > A variant (red circle) occurs at the first intronic base after Exon 2. **(B)** Agarose gel image of minigene splicing assay. HEK293T cells were left untreated (Control) or transfected with WT or c.294 + 1G > A minigenes. The unspliced mRNA (or plasmid DNA) yields 580 bp and the spliced product is 380 bp. **(C)** Agarose gel image of RT-PCR products spanning from exon 1-4 in fibroblasts from the proband and three control samples. The WT transcript amplifies a predicted 322 bp band, while the proband sample produced a 202 bp fragment. **(D)** Chromatogram of the proband amplicon indicating skipping of Exon 2.

yeast based on overexpression studies. This domain is also required for both mating and sterol trafficking in yeast (3). Given the high level of conservation between the AHD between yeast and human *arv1* (44%) (1), it is likely that p.(Lys59_Asn98del) encodes a non-functional protein.

Functional complementation with human ARV1 variants in *Saccharomyces cerevisiae*

We next tested the impact of the previously reported p.(Gly189Arg) (12) and the current p.(Lys59_Asn98del) variants on ARV1 function. Yeast strains deleted for the *arv1* locus are inviable at restrictive growth temperature (37°C), and this temperature sensitivity can be rescued with expression of human *ARV1* (1,6,7). Thus, we sought to determine if Gly189Arg and Lys59_Asn98del variants could also rescue growth and viability in *arv1*Δ yeast. WT and *arv1*Δ yeast were dilution plated and allowed to grow at permissive (30°C) or restrictive (37°C) temperature for 72 h. As previously shown in (1,6,7), *arv1*Δ yeast were inviable at 37°C and could be rescued by overexpression of either ScARV1 or hARV1 (Fig. 4). The Gly189Arg variant showed a partial rescue relative to WT hARV1. In contrast, the Lys59_Asn98del variant completely failed to rescue growth and viability in *arv1*Δ yeast at 37°C.

Protein expression of the p.(Gly189Arg) and p.(Lys59_Asn98del) variants

The glycine residue at position 189 is highly conserved across all mammalian species (Supplementary Material, Figure S4) and resides in a predicted transmembrane domain (via HOPE (15) and CCTOP (16)). Likewise, the p.(Lys59_Asn98del) variant removes a large portion of the highly conserved AHD, and both variants could be deleterious to protein expression or stability. Therefore, we tested the effects of the p.(Gly189Arg) and p.(Lys59_Asn98del) variants on ARV1 protein expression in mammalian cells. Mammalian expression vectors were generated for WT, Gly189Arg, or Lys59_Asn98del ARV1 that include an N-terminal 3XFLAG-HA epitope tag. These constructs were transfected into HEK293T cells, and ARV1 protein levels were measured by western blotting (Fig. 5). A plasmid expressing green fluorescent protein (GFP) was used as a negative control, and a V5 epitope-tagged far-red protein (mKate2) was co-transfected for normalization. WT ARV1 protein was readily detectable with the antibody to the HA epitope tag at the expected 36 kDa molecular weight in lane 2 (Fig. 5). In contrast, neither Gly189Arg hARV1 (36 kDa) nor K59_98Del (31 kDa) could be detected above background (Fig. 5).

Fiber type changes in *Arv1* KO mice

Muscle histology on the proband with the c.294 + 1G > A variant showed an increase in the expected number of Type I oxidative fibers. Mice with a germline deletion of *Arv1* are exceptionally lean and more active (10), and we hypothesized that *Arv1* deficiency may also affect fiber type distribution in mice. We performed immunostaining for myosin heavy chain isoforms to examine fiber type distribution in extensor digitorum longus (EDL), diaphragm, and soleus muscles. Male *Arv1* KO mice, 10 weeks of age, had a significant increase in the relative abundance of Type I fibers in the diaphragm, but no major changes in the other muscles (Supplementary Material, Figure S5). In female *Arv1* KO mice, 14 weeks of age, we saw a similar increase

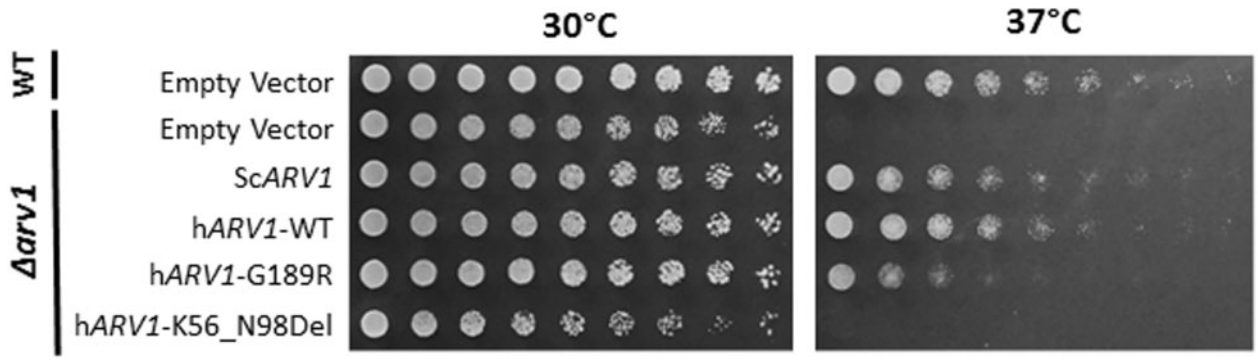

Figure 4. Complementation assay for Gly189Arg and Lys59_Asn98Del variants in yeast. WT and *arv1Δ Saccharomyces cerevisiae* strains were transformed with empty pRS426 (2μ, URA3), or pRS426 containing ScARV1, hARV1, hARV1-G189R, or hARV1-K56_N98Del. Strains were grown to stationary phase, then spotted onto standard Ura3 dropout media in a 1:2 dilution series from 0.1 OD_{600}/mL. Plates were incubated at permissive (30 °C) or restrictive (37 °C) temperature for 72h.

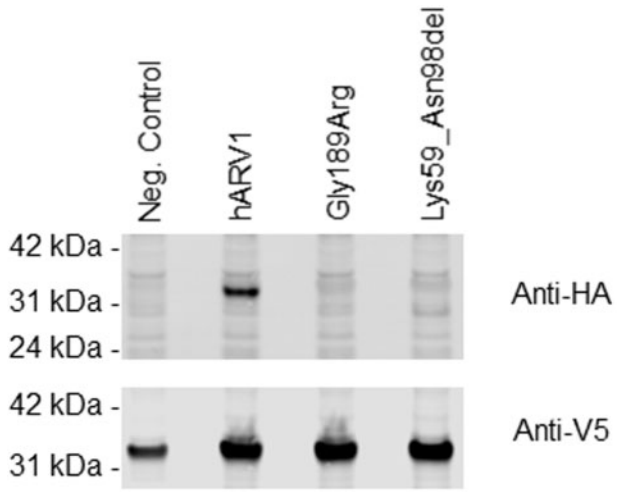

Figure 5. Protein expression of the Gly189Arg and Lys59_Asn98Del variants. Western blot of HEK293T cells transiently transfected with GFP (Neg. Control), WT, Gly189Arg, or Lys59_Asn98Del ARV1 constructs containing an N-terminal 3XFLAG-HA epitope tag, and detected with an anti-HA antibody (top). Cells were co-transfected with mKate2 (red fluorescent protein) which was detected with an anti-V5 antibody as a transfection and loading control (bottom). The expected sizes of epitope tagged ARV1 proteins are: WT and Gly189Arg: 36 kDa, and Lys59_Asn98Del: 31 kDa.

in Type I fibers in the diaphragm but also a dramatic increase in Type I fibers in the EDL (Supplementary Material, Figure S6).

Mice with a neuronal deletion of *Arv1*

Given the severe neurological phenotypes in the individuals with p.(Gly189Arg) and p.(Lys59_Asn98del) we hypothesized that the main site of ARV1 action may be the brain. To test this, we generated mice with a neuronal knockout (NKO) of *Arv1* by breeding mice with a floxed allele (10) (exons 2 and 3) to *Nestin-cre* transgenic mice. To determine the efficiency and specificity of *Arv1* deletion, mRNA levels were measured across nine tissues. There was a 92% decrease in WT *mArv1* mRNA expression in brain (Supplementary Material, Figure S7 A), but no significant decrease in any of the other tissues tested, confirming robust and specific neuronal deletion. We previously found that mice lacking *Arv1* in the germline exhibit a lean phenotype with increased activity and energy expenditure. To test whether loss of *Arv1* in the brain is responsible, *Arv1* NKO mice were maintained on a chow diet and observed weekly through 20 weeks of age. *Nestin-cre* mice have been reported to exhibit a weight phenotype independent of gene deletion (17), so Cre positive $Arv1^{+/+}$ and $Arv1^{+/fl}$ mice were included as controls. Male NKO mice weighed significantly less than control mice beginning at 6 weeks of age, with a 21% decrease in final body weight (P 0.0001) (Fig. 6). Likewise, female NKO mice were significantly lighter from 8 weeks of age, and weighed 15% less at 20 weeks ($P = 0.0003$). White adipose tissue mass was reduced in all depots examined of the male *Arv1* NKO mice (Supplementary Material, Figure S7B), as observed in mice with germline deletion (10). Only perigonadal fat mass was significantly lower in female mice relative to controls (Supplementary Material, Figure S7C).

ARV1 NKO mice have seizures and a survival defect

Both the previously reported individuals (homozygous p.(Gly189Arg)) and the current proband (homozygous c.294 + 1G > A), had a severe neurological condition and seizure disorder. Interestingly, we found that mice with neuronal deletion of *Arv1* often showed circling behavior (Supplementary Material, Video 1) and were prone to seizures. In an extreme example, we documented a seizure in a 20-week-old female mouse that exhibited circling behavior and weight loss in the 2 weeks prior to the event. The generalized tonic-clonic seizure lasted for 15 min before the mouse died in a prone position with rigid flexed muscles (Supplementary Material, Video 2). We observed spontaneous death occurring at 3–5 months of age in the NKO mice, with animals often found in a similar prone position with rigid muscles. This was foreshadowed by a 0.5–2.0 g loss in body weight in the preceding 2-week period. The seizures were not inducible by dissonant sounds, spooking, or strobe light challenge. Although spontaneous seizures are unpredictable and difficult to quantify, we observed a trend towards decreased survival in males, with 80% remaining alive through 20 weeks of observation ($P = 0.26$) (Fig. 6C). Female *Arv1* NKO mice had a severe survival defect, with only 33% of mice surviving to 20 weeks ($P = 0.0053$) (Fig. 6D).

Discussion

Here, we describe an individual with a severe early infantile epileptic encephalopathy (EIEE) who died at 12 months of age. Homozygosity mapping and exome sequencing identified a homozygous splice site variant (c.294 + 1G > A) in the *ARV1* gene in

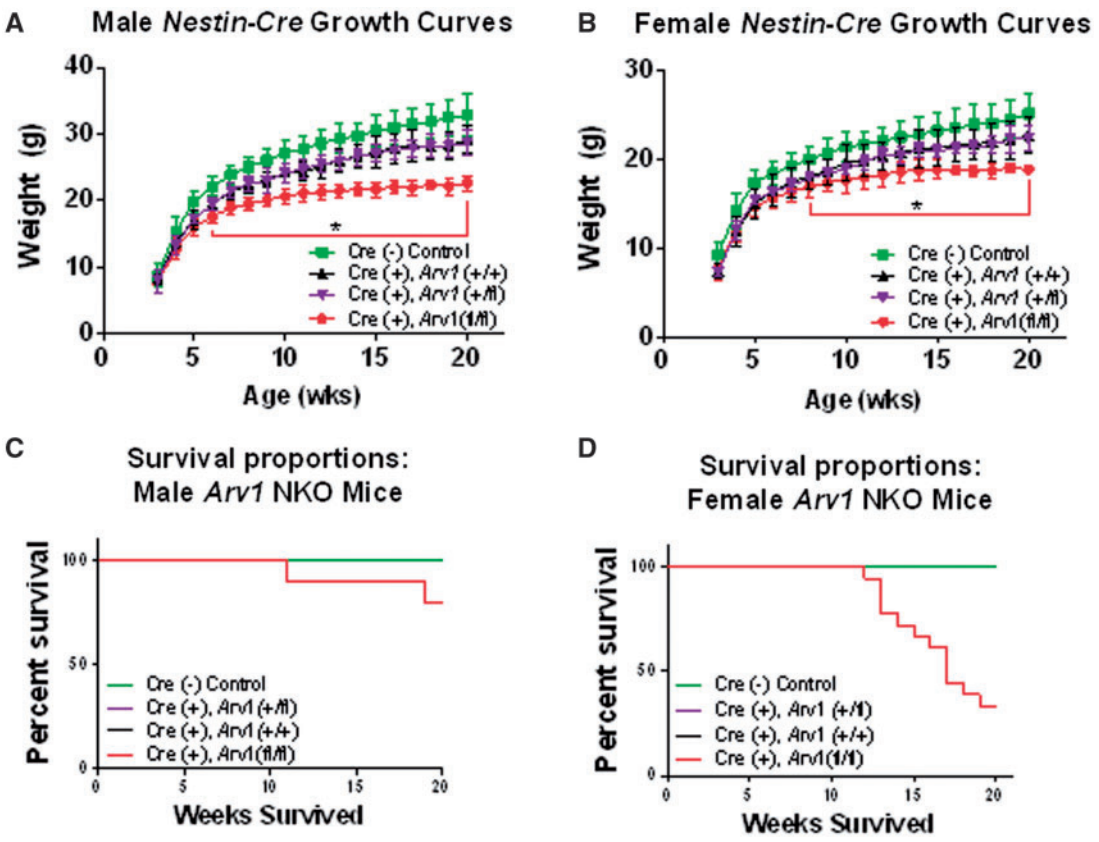

Figure 6. Growth and survival of *Arv1* NKO mice. Mice were maintained on a standard chow diet and weighed weekly beginning at weaning (3 weeks) through 20 weeks of age. **(A)** Male growth curves: Cre^{-} Control ($n=28$–34); $Cre^{+}Arv1^{+/+}$ ($n=6$–12); $Cre^{+}Arv1^{+/fl}$ ($n=4$–9); $Cre^{+}Arv1^{fl/fl}$ ($n=7$–12). **(B)** Female growth curves: Cre^{-} Control ($n=23$–31); $Cre^{+}Arv1^{+/+}$ ($n=8$–9); $Cre^{+}Arv1^{+/fl}$ ($n=5$–6); $Cre^{+}Arv1^{fl/fl}$ ($n=6$–20). Survival was tracked from birth through 20 weeks of age. No spontaneous deaths were observed in the control genotypes for males or females. **(C)** Male survival curves. By 20 weeks of age, 20% of male $Cre^{+}Arv1^{fl/fl}$ mice spontaneously died: Cre^{-} Control ($n=18$); $Cre^{+}Arv1^{+/+}$ ($n=6$); $Cre^{+}Arv1^{+/fl}$ ($n=9$); $Cre^{+}Arv1^{fl/fl}$ ($n=10$); Mantel-Cox Log-rank test $p=0.073$. **(D)** Female survival curves. By 20 weeks of age, 67% of $Cre^{+}Arv1^{fl/fl}$ female mice spontaneously die: Cre^{-} Control ($n=17$); $Cre^{+}Arv1^{+/+}$ ($n=8$); $Cre^{+}Arv1^{+/fl}$ ($n=5$); $Cre^{+}Arv1^{fl/fl}$ ($n=18$); Mantel-Cox Log-rank test $P=0.0053$. Data in panels A and B are mean ± SD.

the proband, while both unaffected parents were heterozygous for this variant. The candidacy of *ARV1* as the causal gene in this patient was supported by our recent report of a similarly affected individual homozygous for a non-conservative amino acid change in *ARV1* (p.(Gly189Arg)) (12). Two additional similarly affected relatives have been confirmed with the same genotype. Although the proband with the p.(Lys59_Asn98del) variant had a more severe clinical phenotype than the affected individuals with p.(Gly189Arg), there are many shared clinical features including intractable EIEE (5/5), severe-profound intellectual disability/developmental delay (5/5), movement disorder (3/5), visual impairment (2/5) and premature death (2/5) (Supplementary Material, Table S2). It will be important to report the phenotype of additional affected individuals to more precisely define the phenotypic-genotypic spectrum for ARV1-deficiency. Phenotypic intra- and interfamilial variability is common in monogenic neurocognitive disorders; most likely reflecting distinct molecular mechanisms, and additional genetic, epigenetic, and environmental influences on neurodevelopmental pathways (18,19).

We tested the pathogenicity of the newly identified *ARV1* splice site variant (ARV1_NM_022786.1: c.294 + 1G > A; NP_073623.1:p. (Lys59_Asn98del)) using a minigene assay and cloning of the transcript from primary human fibroblasts. This variant abolishes normal splicing, resulting in an in-frame deletion of exon 2 (p.(Lys59-Asn98del)). The predicted truncated protein eliminates a large portion of the N-terminal zinc binding motif in the AHD, including one of the four essential cysteines. Expression of the p.(Lys59-Asn98del) variant completely failed to rescue temperature sensitivity in *arv1*Δ yeast (Fig. 4). Furthermore, this variant did not express detectable levels of ARV1 protein in mammalian cells (Fig. 5), and therefore, is most likely a null allele. The AHD is known to be a critical region of the ARV1 protein that is highly conserved across eukaryotes (44% identity yeast and human). This domain is required to rescue numerous defects in *arv1*Δ yeast including growth at 37°C or under anaerobic conditions (1), susceptibility to sterol-binding antibiotics (1,4,11), shmoo formation for mating (3), and hypersensitivity to inhibitors of sterol synthesis (4,11). Functional complementation with human *ARV1* (1,6,7), as well as the severe phenotype of the current proband, supports an important role for this critical region in human ARV1 function.

We also investigated the effects of the previously reported p.(Gly189Arg) variant on ARV1 function and protein expression. This glycine residue is highly evolutionarily conserved (down to *Caeborhabditis elegans*) and mutation of this region was predicted to be pathogenic by multiple *in silica* tools (SIFT (20), Polyphen2 (21), CADD (22)). Topology mapping in CCTOP (16) (accessed 11 December 2015) placed this glycine in a transmembrane domain in all models. Glycine to arginine is a non-conservative change,

and could conceivably disrupt the transmembrane domain where it is predicted to reside. Interestingly, we found that the p.(Gly189Arg) variant can partially rescue growth at 37°C in *arv1Δ* yeast, but was less effective than WT human ARV1. However, p.(Gly189Arg), like p.(Lys59-Asn98del), did not express detectable levels of ARV1 protein in mammalian cells. Taken together, these data indicate that p.(Gly189Arg) is at least a hypomorph, while p.(Lys59_Asn98del) is most likely a true null. This is logical given the clinical phenotypes of these individuals. Those with the p.(Gly189Arg) variant were less severely affected than the current proband with the p.(Lys59_Asn98del) variant, who died with a severe degenerative condition at 12 months of age (Supplementary Material, Table S2).

The muscle fiber type changes in the proband (c.294 + 1G > A; Lys59_Asn98del), were also seen in mice with germline deletion of *Arv1*. An increased proportion of Type I fibers in the diaphragm was observed in both male and female mice. However, the abundance of Type I fibers in the EDL of female *Arv1* NKO mice is particularly noteworthy. Such a high percentage of slow twitch Type I fibers is extremely rare in this highly glycolytic muscle. It is possible that these fibers failed to undergo the normal developmental switch from Type I to Type II (23). However, this may instead be a consequence of increased locomotor activity or altered neuronal signaling to the muscle caused by absence of *Arv1* in the CNS, since similar reprogramming can be achieved with chronic low frequency electrical stimulation of glycolytic muscles (24,25).

We recently reported that mice with a germline deletion of the *Arv1* gene had a lean phenotype with dramatically lower fat mass and improved glucose tolerance, although the tissue/site of action was unknown (10). Mice with a neuronal deletion of *Arv1* (NKO) also had a lean phenotype and failed to gain weight in adulthood (Fig. 5). Interestingly, these NKO mice were markedly more active, exhibiting circling behavior and hyperactivity (Supplementary Material, Video 1). Like the patients with homozygous variants in *ARV1*, the *Arv1* NKO mice also had seizures (Supplementary Material, Video 2), typically beginning after 12 weeks of age. A large fraction of these mice died unexpectedly in adulthood between 12 and 20 weeks of age. Interestingly, the survival defect was far greater in the female animals, suggesting sexual dimorphism in the phenotype. The reasons for this are still unclear, however differences in phenotypic severity between male and female mice in acquired and genetic models of seizures has been previously noted in (26,27). The lean phenotype of the *Arv1* mice is quite puzzling, as this is rarely a feature of EIEE in humans. In mouse models, it has been shown that deletion of G-protein γ3-subunit (*Gng3*) produces a lean phenotype and seizures (28,29), but unlike the *Arv1* NKO mice, these mice are not hyperactive and the seizures can be induced by audiogenic stimuli. Further work is needed to understand the specific neuronal population(s) impacted by *Arv1* deficiency, and its biochemical role in these neurons. Although outside the scope of this manuscript, these mice could be useful in identifying networks and pathways regulating lipid membrane homeostasis that rely upon ARV1 activity.

EIEE is a devastating group of monogenic disorders with severe and overlapping clinical phenotypes (30). Many studies suggest that the majority of diagnosed cases are due to *de novo* mutations in autosomal or X linked genes (31,32); however, a growing number of autosomal and X-chromosome linked recessive causes are now identified, and a recent study suggests that autosomal and X-linked recessive inheritance may explain approximately 10% of all cases of epileptic encephalopathy (33), which has critical implications for accurate genetic counseling. Many of these genes have known or suspected roles in organic anion transport (34–36), cell signaling (37–40), or vesicular transport (41–43). Although the molecular function of mammalian ARV1 is unknown, it is worth noting that it is required for normal membrane structure and lipid egress from the ER in yeast (1,2,6,8). Even subtle alterations in subcellular membrane lipid composition could have a major impact on synaptic vesicle release as well as membrane depolarization in neurons. In yeast, *ARV1* genetically interacts with enzymes involved in the GPI anchor synthesis (6). ARV1 has been hypothesized to act either as a flippase in the steps preceding GPI anchor synthesis, or in presenting Glucosaminyl-acylphosphatidylinositol (GlcN-acylPI) to PIGM (phosphatidylinositol glycan anchor biosynthesis class M) (6,7). A potential involvement of the GPI anchor pathway is interesting given that homozygous loss of PIGM is associated with absence seizures in humans (44) (MIM 610293), and hemizygous mutation of PIGA (45) and homozygous mutation of PIGQ (46) have been associated with early onset epileptic encephalopathy (MIM 330868 and MIM 605754, respectively).

Still, the exact biochemical function of ARV1 remains elusive, despite intensive research in yeast (1–9,11,47,48). Its absence in this organism results in a panoply of growth and viability defects (1,2,5,6), alterations in lipid synthesis and trafficking (1,2,6), ER stress (8), and impaired autophagy (48). However, until now there has not been a definitive link to a genetic syndrome resulting from deficiency of *ARV1* in humans. We found that both the current (c.294 + 1G > A; Lys59_Asn98del) and previously reported in (12) (p.(Gly189Arg)) variants are functionally defective in yeast, and express undetectable levels of ARV1 protein in mammalian cells. The seizures observed in the NKO mice confirm that mammalian ARV1 plays a critical role in neuronal function. Collectively, our data support deficiency of ARV1 as a cause of EIEE in humans. We propose that *ARV1* should be included in panels for early onset neurocognitive impairment and epileptic encephalopathy.

Materials and Methods

Subjects

The proband was enrolled, with her parents, in a trio exome sequencing project performed at the South East Area Laboratory Services (SEALS) Genetics laboratory as part of a cohort of 31 patients with epileptic encephalopathy, coordinated by the Departments of Clinical Genetics and Paediatric Neurology at Sydney Children's Hospital as previously described in (12,49). Informed consent for exome sequencing was obtained and the research was approved by the ethics committee from The Sydney Children's Hospital Network and the Prince of Wales Hospital Campus, Sydney, Australia (HREC ref no 13/094 and LNR/13/SCHN/112).

Exome sequencing and Sanger confirmation

High-quality DNA was obtained by extraction from peripheral blood in EDTA. Next Generation Sequencing was performed using an Ampliseq exome kit, with libraries sequenced on a Life Technologies Proton instrument using a P1 v2 chip. Reads were aligned to Human Genome Reference Sequence Hg19/GRCh37 using map aligner and then an in-house downstream pipeline. Data filtering and variant prioritization were performed using the GEMINI platform as described previously in (49). Bidirectional Sanger sequencing was performed on DNA from the proband, both parents, and two healthy siblings using

standard methodology to verify and segregate candidate variants. The variant was submitted to the publically available data base ClinVar http://www.ncbi.nlm.nih.gov/clinvar/, last accessed May 2016 (accession number SCV000262756).

Muscle histology and electron microscopy

An open biopsy of quadriceps muscle was sampled from the patient at 7 months of age. Paraffin and frozen sections were cut and stained with H&E, myosin ATPase stains (standard and reverse ATPase stains, blue ATPase stain), gomori trichrome, acid phosphatase, mitochondrial stains (succinate dehydrogenase and combined cytochrome C/succinate dehydrogenase), PAS and fat stains. Blue myosin ATPase is a method developed in-house similar to standard ATPase stains, but using a metachromatic blue dye which does not fade with time, unlike standard ATPase stains. A portion of the biopsy was fixed in 2.5% glutaraldehyde in 0.1 M sodium cacodylate buffer pH7.4 and processed routinely for electron microscopy. Ultra-thin sections were contrast stained with uranyl acetate and lead citrate and examined in an FEI Tecnai Spirit Biotwin transmission electron microscope.

Generation of hArv1 minigene and expression vectors

The human *ARV1* genomic reference sequence (GRCh38.p2, NC000001.11: 230979075-231000733) and associated *ARV1* cDNA sequence (GenBank accession number AF290878.1) were used to design the vectors used in this study. To test the splicing variant c.294 + 1G > A, we generated wild-type and variant minigene constructs containing an N-terminal HA tag fused to *hArv1* exon 2, the first and last 100 bp of intron 2, and *hArv1* exon 3 as gBlocks (Integrated DNA Technologies) for direct cloning into pEYFP-N1 (Clontech) in frame with the EYFP protein, as shown in Figure 3. Forward primer KEJ_0032: CTA CCG GAC TCA GAT CTC GAG CTC, and reverse primer KEJ_0033: CTC ACC ATG GTG GCG ACC GGT G were used to amplify the 580 bp fragments for cloning. PCR amplicons were then digested with SacI and BamHI and cloned into pEYFP-N1 with the same enzymes to generate plasmids 1303_pMini-hARV1-Exon2-3-WT-EYFP and 1304_pMini-hARV1-Exon2-3-Mut-294p1GtoA-EYFP, encoding the wild-type and variant minigene cassettes respectively. In order to examine protein stability for the p.(Gly189Arg) (c.565G > A) variant (12), we used the mammalian expression vector 1010_p3XFLAG-HA-CMV-7.1, a derivative of P3XFLAG-CMV-7.1, which was obtained from Sigma-Aldrich. To make p3XFLAG-HA-CMV-7.1, complementary oligonucleotides encoding the hemagglutinin (HA) tag were ordered from IDT: Top-AGC TTT ACC CAT ACG ATG TTC CAG ATT ACG CTA CGC GTG; Bottom- AAT TCA CGC GTA GCG TAA TCT GGA ACA TCG TAT GGG TAA. These oligos were annealed and then ligated into P3XFLAG-CMV-7.1 that was linearized with HindIII and EcoRI. The resulting vector, 1010_p3XFLAG-HA-CMV-7.1 encodes a 3XFLAG-HA tag followed by a novel MluI site in frame with the original multicloning site. We then generated gBlocks containing the entire wild-type or variant cDNA sequence for cloning that included different 5′ restriction sites to allow inclusion or removal of the 3XFLAG-HA tag in the final product. The forward primer KEJ_0034: ATA TAA GCA GAG CTC GTT TAG TGA ACC GTC and reverse primer KEJ_0035: GTC ACA GGG ATG CCA CCC GGG ATC were used to PCR amplify the 899 bp gblocks. PCR amplicons were digested with SacI and BamHI and ligated into 1010_p3XFLAG-HA-CMV-7.1 digested with the same enzymes to produce 1307_pCMV-hARV1-WT and 1308_pCMV-hARV1-G189R encoding the native wild-type and p.(Gly189Arg) variants respectively. The same PCR products were digested with EcoRI and BamHI and ligated into 1010_p3XFLAG-HA-CMV-7.1 digested with the same enzymes to produce 1309_pCMV-3xFLAG-HA-hARV1-WT and 1310_pCMV-3xFLAG-HA-hARV1-G189R, the 3XFLAG-HA tagged versions respectively. Finally, the finalized inserts in these vectors were amplified by PCR to generate 848 bp products for the untagged hARV1 variants and 969 bp products for the 3xFLAG-HA-ARV1 variants and then digested with NheI and AgeI. These were ligated into a pUC57 vector containing the CB promoter, SV40 chimeric intron, and bovine growth hormone polyadenylation signal that was synthesized by Genewiz to generate 1322_pUC57-CB-hARV1-WT-BGH-pA, 1323_pUC57-CB-hARV1-G189R-BGH-pA, 1324_pUC57-3XF-HA-hARV1-WT-BGH-pA, and 1325_pUC57-3XF-HA-hARV1-G189R-BGH-pA. To generate native and 3xFLAG-HA tagged p.Lys59_Asn98Del variant expression constructs, 1322_pUC57-CB-hARV1-WT-BGH-pA and 1324_pUC57-3XF-HA-hARV1-WT-BGH-pA were cut with BsaBI and Bsu36. Complementary oligonucleotides (KEJ_0050: CCA TCT GTA TCC ATG GAA AAC TCT GCA TAT TTT GTT TGC TTT GTG AAG CAT ACC and KEJ_0051: TCA GGT ATG CTT CAC AAA GCA AAC AAA ATA TGC AGA GTT TTC CAT GGA TAC AGA TGG) were annealed and ligated into the cut vectors to generate 1336_pUC57-CB-hARV1-exon2-SKIP-BGH-pA and 1337_pUC57-CB-3xFLAG-HA-hARV1-exon2-SKIP-BGH-pA. For yeast expression, the pRS426-GPD-empty plasmid was used, which contains the yeast *GPD* promoter and *CYC1* terminator. To generate yeast expression vectors for WT, Gly189Arg, and Lys59_Asn98Del variants, the respective hARV1 coding sequences were PCR amplified using the primers KEJ_0054: CTG CAG GAA TTC GAT ATG GGC AAC GGC GGG CGG AG and KEJ_0056: GAC TCG AGG TCG ACT CAG AAG TCC TGA GAT TTA AAG ATG from plasmids 1322_pUC57-CB-hARV1-WT-BGH-pA (825 bp), 1323_pUC57-CB-hARV1-G189R-BGH-pA (825 bp), and 1336_pUC57-CB-hARV1-exon 2 SKIP-BGH-pA (705 bp). The resulting PCR products were digested with EcoRI and SalI and ligated into pRS426-GPD-Empty cut with the same enzymes to generate 1356_pRS426-GPD-hARV1-WT-CYC1, 1357_pRS426-GPD-hARV1-G189R-CYC1, and 1358_pRS426-GPD-hARV1-delExon2-CYC1. All clones were verified by Sanger sequencing at Lone Star Laboratories (Houston, TX).

Cell culture and transfection

HEK 293T cells were obtained from the American Type Tissue Collection and cultured in standard growth media (10% fetal bovine serum (FBS), 2 mM L-glutamine, 100 U/ml penicillin/streptomycin in Dulbecco's Modified Eagle Medium). HEK 293T cells were plated in 6-well plates (Greiner) and transfected using polyethylenimine (PEI) (50) with 1.3 μg plasmid DNA per well at a 4:1 ratio of PEI to DNA in six-well tissue culture dishes. Cells were directly harvested for western in LDS buffer (Life Technologies) or harvested by scraping in ice cold PBS and frozen at -80 degrees prior to RNA extraction.

Minigene assay and quantitative reverse transcriptase PCR (qRT-PCR)

Following harvest, RNA was isolated from cells via Qiagen RNeasy kit with on-column Dnase digestion to remove transfected plasmid. RNA (1 μg) was reverse transcribed (iScript Reverse Transcriptase, BioRad) and diluted prior to PCR. Primers

KEJ_0032 (CTA CCG GAC TCA GAT CTC GAG CTC) and KEJ_0033 (CTC ACC ATG GTG GCG ACC GGT G) were used to amplify spliced (380 bp) and unspliced (580 bp) products from 2.5 ng cDNA through 25 cycles of PCR. The final PCR products were separated on a 2% agarose gel stained with ethidium bromide. RNA was isolated from brain, white adipose tissue, and brown adipose tissue with the Qiagen RNeasy Lipid Tissue Mini Kit, and the RNeasy Mini Kit was used for all other tissues. One microgram of RNA (0.5 μg for diaphragm) was reverse transcribed (iScript, BioRad) and diluted 1:5 prior to quantitative PCR (qPCR) analysis. Taqman probes to mArv1 (Mm01253489_m1, Life Technologies) and mβActin (4352933E, Life Technologies) were used to amplify 4 μl diluted cDNA in triplicate. Samples from qPCR were analyzed by the ΔΔcT method (51) and graphed in GraphPad Prism 6.

Primary fibroblasts

Primary fibroblasts were isolated from a skin biopsy taken from the proband pre-mortem using standard methodology (52). The cells were grown in 25 cm^2 tissue culture flasks in Minimum Essential Eagle's Media (Sigma 5650) supplemented with 15% (FBS, Sigma 26140079), 2 mM L-Glutamine (Gibco BRL 25030-163), and 1% antibiotic/antimycotic in a humidified incubator with 5% CO_2. Total RNA was isolated from cells at passage 4 using the QIAamp Blood mini kit (QIAGEN) according to the manufacturer's instructions. One microgram of RNA was reversed transcribed into cDNA using oligo dT primers and the M-MLV reverse transcriptase (Promega).

Sequencing of ARV1 splice variant mRNA

Total RNA (1 μg) from the proband's primary fibroblasts or three control donors was reversed transcribed into cDNA using oligo dT primers and the M-MLV reverse transcriptase (Promega). Primers specific to exons 1 and 4 (Fwd-ex1: GGTGTGCT GAAGATAACCATCTG, Rev2-ex4: TGCCAATAAAATAGGCAGT TTGT) were used to amplify a predicted 322 bp fragment spanning the NM_022786.1:c.294 + 1G > A variant and surrounding exons with HotStarTaq polymerase (QIAGEN). PCR products were separated on a 2% agarose gel. The truncated amplicon from the proband (~202 bp) was extracted from the gel and subjected to Sanger sequencing using the PCR primers listed above.

Western blotting

HEK293T cells were harvested in 1 ml LDS Buffer (Life Technologies) and supplemented with beta-mercaptoethanol to 5% final (v/v), denatured by heating to 95 °C for 5 min, and allowed to cool before separation by SDS-PAGE on 4-15% NuPage Bis Tris Gels with MES running buffer (Life Technologies). Two percent of the total lysate (20 μl) was separated per well. Proteins were then transferred to nitrocellulose membranes and blocked in a 2:1 ratio of Odyssey Blocking Buffer (LiCor) and PBS plus 0.05% Tween-20 for 1 h. Primary antibodies were applied overnight in PBS plus 0.05% Tween-20 and 1% bovine serum albumin at 4° for mouse anti-Beta Tubulin (E-7, University of Iowa Developmental Studies Hybridoma Bank) mouse anti-V5 (R96025, Life Technologies), rabbit anti-ARV1 (ARP49756_P050, Aviva), and rabbit anti-HA tag (sc-105, Santa Cruz). Membranes were incubated with DyLight goat anti-rabbit 680 nm and goat anti-mouse 800 nm fluorescent secondary antibodies (6111440020 and 6101450020, Rockland Immunochemicals) for 1 h at room temperature and then imaged with an Odyssey CL Imager (LiCor).

Yeast complementation studies

Saccharomyces cerevisiae WT strain FK113 (*MATα*, *his3, lys2, leu2, trp1, ura3, bar1-1*) and *arv1Δ* strain FK137 (*MATα*, *his3, lys2, leu2, trp1, ura3, bar1-1, arv1Δ::TRP1*) were previously described in (6,7). Parental WT FK113 and KO FK137 strains were maintained in YPD media (Fisher, BP2469-500). Yeast were chemically transformed with empty vector, or yeast or human ARV1 variant expression constructs to obtain individual clones using standard methodology (6,7,53), Transformed strains were maintained in synthetic Ura-dropout media (Clontech, ST0045). To perform temperature sensitivity assays, transformed strains were incubated at 25°C and 200 RPM until stationary phase was reached. All clones were diluted to 0.1 OD_{600}/ml, and serially diluted 1:2 prior to spotting. Ten microliters of each dilution were spotted on each duplicate plate and incubated at 30 or 37°C for 72 h.

Animal studies

All mouse studies were completed with approval of the Institutional Animal Care and Use Committee of Baylor College of Medicine (protocol AN-6243). A light cycle of 14-h light and 10-h dark was maintained for the duration of the studies. Mice were group housed with littermates and provided with a standard chow diet, *ad libitum*. The mice were weighed weekly from weaning through 20 weeks of age. Growth curves were analyzed by grouped *t*-test at each weekly time point and graphed in GraphPad Prism 6. Circling behavior, barbering, seizures, and spontaneous death were recorded as they were observed. At 20 weeks of age, mice were euthanized, and tissues were collected, weighed, and stored for future analysis. Final 20-week tissue and body weights differences were assessed by unpaired *t*-test both by weight and by percentage body weight. Survival analysis was completed via Log-rank (Mantel-Cox) test and incudes survival data up to 20 weeks of age.

Fiber typing of murine muscles

Mouse skeletal muscles were embedded in OCT compound (Tissue Tek) and rapidly frozen in isopentane cooled in a bath of liquid nitrogen. The frozen muscles were sectioned to a 10 micron thickness and subjected to immunofluorescence staining exactly as previously described in (54). Myosin heavy chain antibodies were obtained from the University of Iowa-Developmental Studies Hybridoma Bank: mouse anti-Myosin heavy chain I (BA-F8 IgG_{2b}), mouse anti-Myosin heavy chain IIa (SC-71, IgG_1). Fluorescent secondary antibodies were obtained from Fisher Scientific: Goat anti-Mouse IgG2b, Alexa Fluor 594 (A21145) and Goat anti-Mouse IgG1, Alexa Fluor 488 (A21121).

Generation of NKO mice

Conditional mice with a floxed allele for *Arv1* (exons 2 and 3) were bred to mice expressing the *Nestin-cre* transgene (B6.Cg-Tg(Nes-Cre)1Kln/J, Jackson Laboratories) to obtain mice that were $Arv1^{fl/fl}$ and expressed *Nestin-cre*, referred to as NKO Mice. There were no phenotypic differences noted between *Cre*-negative mice with *Arv1* genotypes of (+/+), (+/fl), or (fl/fl), and these are collectively referred to as 'Control' animals in the results. This *Cre* deletes in both the central and peripheral

nervous system, but may leak in the germline (17). In this case, no female NKO mice produced pups, so all breedings required use of *Cre*-positive males. Mice were genotyped at weaning from tail clips for the *Arv1* WT, floxed, and null alleles, as well as the *Nestin-cre* transgene, as previously described in (10). Because liver is known to be a tissue where *Nestin-cre* is not expressed (17,55), this tissue was genotyped after experimental endpoints to ensure that *Arv1* was not deleted in the germline or early embryonic development.

Supplementary Material

Supplementary Material is available at *HMG* online.

Acknowledgements

The authors would like thank the patients' families for their participation in this study, the clinical neurology, general pediatric and clinical genetics teams involved with the clinical care and support of the patients and the expert technical assistance of Toni Saville, Glenda Mullan, William Lo and Corrina Walsh from SEALS Genetics Laboratory and Elena Rumyantseva and Chris Tesoriero from SEALS Anatomical Pathology laboratory. Finally, we would like to thank Laramie Lemon from Baylor College of Medicine for technical assistance with the yeast studies.

Conflict of Interest statement. None declared.

Funding

This work was supported by the American Heart Association [16BGIA26420102 to W.R.L.]; the National Institutes of Health [5 T32 GM008231 to K.E.J. via the Integrative Molecular and Biomedical Sciences Graduate Program]; King Abdulaziz City for Science and Technology [13-BIO1113-20 to F.S.A.]; and the National Health and Medical Research Council [GNT11149630 to E.P., GNT0512123 to T.R.].

References

1. Tinkelenberg, A.H., Liu, Y., Alcantara, F., Khan, S., Guo, Z., Bard, M. and Sturley, S.L. (2000) Mutations in yeast ARV1 alter intracellular sterol distribution and are complemented by human ARV1. *J. Biol. Chem.*, **275**, 40667–40670.
2. Swain, E., Stukey, J., McDonough, V., Germann, M., Liu, Y., Sturley, S.L. and Nickels, J.T. Jr. (2002) Yeast cells lacking the ARV1 gene harbor defects in sphingolipid metabolism. Complementation by human ARV1. *J. Biol. Chem.*, **277**, 36152–36160.
3. Villasmil, M.L., Ansbach, A. and Nickels, J.T. Jr. (2011) The putative lipid transporter, Arv1, is required for activating pheromone-induced MAP kinase signaling in Saccharomyces cerevisiae. *Genetics*, **187**, 455–465.
4. Gallo-Ebert, C., McCourt, P.C., Donigan, M., Villasmil, M.L., Chen, W., Pandya, D., Franco, J., Romano, D., Chadwick, S.G., Gygax, S.E., *et al.* (2012) Arv1 lipid transporter function is conserved between pathogenic and nonpathogenic fungi. *Fungal Genet. Biol.*, **49**, 101–113.
5. Ruggles, K.V., Garbarino, J., Liu, Y., Moon, J., Schneider, K., Henneberry, A., Billheimer, J., Millar, J.S., Marchadier, D., Valasek, M.A. *et al.* (2014) A functional, genome-wide evaluation of liposensitive yeast identifies the "ARE2 required for viability" (ARV1) gene product as a major component of eukaryotic fatty acid resistance. *J. Biol. Chem.*, **289**, 4417–4431.
6. Kajiwara, K., Watanabe, R., Pichler, H., Ihara, K., Murakami, S., Riezman, H. and Funato, K. (2008) Yeast ARV1 is required for efficient delivery of an early GPI intermediate to the first mannosyltransferase during GPI assembly and controls lipid flow from the endoplasmic reticulum. *Mol. Biol. Cell*, **19**, 2069–2082.
7. Ikeda, A., Kajiwara, K., Iwamoto, K., Makino, A., Kobayashi, T., Mizuta, K. and Funato, K. (2016) Complementation analysis reveals a potential role of human ARV1 in GPI anchor biosynthesis. *Yeast*, **33**, 37–42.
8. Shechtman, C.F., Henneberry, A.L., Seimon, T.A., Tinkelenberg, A.H., Wilcox, L.J., Lee, E., Fazlollahi, M., Munkacsi, A.B., Bussemaker, H.J., Tabas, I. *et al.* (2011) Loss of subcellular lipid transport due to ARV1 deficiency disrupts organelle homeostasis and activates the unfolded protein response. *J. Biol. Chem.*, **286**, 11951–11959.
9. Georgiev, A.G., Johansen, J., Ramanathan, V.D., Sere, Y.Y., Beh, C.T. and Menon, A.K. (2013) Arv1 regulates PM and ER membrane structure and homeostasis but is dispensable for intracellular sterol transport. *Traffic*, **14**, 912–921.
10. Lagor, W.R., Tong, F., Jarrett, K.E., Lin, W., Conlon, D.M., Smith, M., Wang, M.Y., Yenilmez, B.O., McCoy, M.G., Fields, D.W. *et al.* (2015) Deletion of murine Arv1 results in a lean phenotype with increased energy expenditure. *Nutr. Diab.*, **5**, e181.
11. Villasmil, M.L. and Nickels, J.T. Jr. (2011) Determination of the membrane topology of Arv1 and the requirement of the ER luminal region for Arv1 function in Saccharomyces cerevisiae. *FEMS Yeast Res.*, **11**, 524–527.
12. Alazami, A.M., Patel, N., Shamseldin, H.E., Anazi, S., Al-Dosari, M.S., Alzahrani, F., Hijazi, H., Alshammari, M., Aldahmesh, M.A., Salih, M.A. *et al.* (2015) Accelerating novel candidate gene discovery in neurogenetic disorders via whole-exome sequencing of prescreened multiplex consanguineous families. *Cell Rep.*, **10**, 148–161.
13. Gillespie, F.D. (1966) Congenital amaurosis of Leber. *Am. J. Ophthalmol.*, **61**, 874–880.
14. Chung, D.C. and Traboulsi, E.I. (2009) Leber congenital amaurosis: clinical correlations with genotypes, gene therapy trials update, and future directions. *J. Aapos*, **13**, 587–592.
15. Venselaar, H., Te Beek, T.A., Kuipers, R.K., Hekkelman, M.L. and Vriend, G. (2010) Protein structure analysis of mutations causing inheritable diseases. An e-Science approach with life scientist friendly interfaces. *BMC Bioinformatics*, **11**, 548.
16. Dobson, L., Remenyi, I. and Tusnady, G.E. (2015) CCTOP: a Consensus Constrained TOPology prediction web server. *Nucleic Acids Res.*, **43**, W408–W412.
17. Harno, E., Cottrell, E.C. and White, A. (2013) Metabolic pitfalls of CNS Cre-based technology. *Cell Metab.*, **18**, 21–28.
18. Stamberger, H., Nikanorova, M., Willemsen, M.H., Accorsi, P., Angriman, M., Baier, H., Benkel-Herrenbrueck, I., Benoit, V., Budetta, M., Caliebe, A. *et al.* (2016) STXBP1 encephalopathy: A neurodevelopmental disorder including epilepsy. *Neurology*, **86**, 954–962.
19. Digilio, M.C., Angioni, A., De Santis, M., Lombardo, A., Giannotti, A., Dallapiccola, B. and Marino, B. (2003) Spectrum of clinical variability in familial deletion 22q11.2: from full manifestation to extremely mild clinical anomalies. *Clin. Genet.*, **63**, 308–313.
20. Ng, P.C. and Henikoff, S. (2001) Predicting deleterious amino acid substitutions. *Genome Res.*, **11**, 863–874.

21. Adzhubei, I.A., Schmidt, S., Peshkin, L., Ramensky, V.E., Gerasimova, A., Bork, P., Kondrashov, A.S. and Sunyaev, S.R. (2010) A method and server for predicting damaging missense mutations. *Nat Methods*, **7**, 248–249.
22. Kircher, M., Witten, D.M., Jain, P., O'Roak, B.J., Cooper, G.M. and Shendure, J. (2014) A general framework for estimating the relative pathogenicity of human genetic variants. *Nat. Genet.*, **46**, 310–315.
23. Hagiwara, N., Yeh, M. and Liu, A. (2007) Sox6 is required for normal fiber type differentiation of fetal skeletal muscle in mice. *Dev. Dyn.*, **236**, 2062–2076.
24. Serrano, A.L., Murgia, M., Pallafacchina, G., Calabria, E., Coniglio, P., Lomo, T. and Schiaffino, S. (2001) Calcineurin controls nerve activity-dependent specification of slow skeletal muscle fibers but not muscle growth. *Proc. Natl. Acad. Sci. USA*, **98**, 13108–13113.
25. Wehrle, U., Dusterhoft, S. and Pette, D. (1994) Effects of chronic electrical stimulation on myosin heavy chain expression in satellite cell cultures derived from rat muscles of different fiber-type composition. *Differentiation*, **58**, 37–46.
26. Twele, F., Tollner, K., Brandt, C. and Loscher, W. (2016) Significant effects of sex, strain, and anesthesia in the intrahippocampal kainate mouse model of mesial temporal lobe epilepsy. *Epilepsy Behav.*, **55**, 47–56.
27. Scharfman, H.E. and MacLusky, N.J. (2014) Sex differences in the neurobiology of epilepsy: a preclinical perspective. *Neurobiol. Dis.*, **72 Pt B**, 180–192.
28. Schwindinger, W.F., Borrell, B.M., Waldman, L.C. and Robishaw, J.D. (2009) Mice lacking the G protein gamma3-subunit show resistance to opioids and diet induced obesity. *Am. J. Physiol. Regul. Integr. Comp. Physiol.*, **297**, R1494–R1502.
29. Schwindinger, W.F., Giger, K.E., Betz, K.S., Stauffer, A.M., Sunderlin, E.M., Sim-Selley, L.J., Selley, D.E., Bronson, S.K. and Robishaw, J.D. (2004) Mice with deficiency of G protein gamma3 are lean and have seizures. *Mol. Cell Biol.*, **24**, 7758–7768.
30. McTague, A., Howell, K.B., Cross, J.H., Kurian, M.A. and Scheffer, I.E. (2016) The genetic landscape of the epileptic encephalopathies of infancy and childhood. *Lancet Neurol.*, **15**, 304–316.
31. Euro, E.R.E.S.C., Epilepsy Phenome/Genome, P. and Epi, K.C. (2014) De novo mutations in synaptic transmission genes including DNM1 cause epileptic encephalopathies. *Am. J. Hum. Genet.*, **95**, 360–370.
32. Epi, K.C., Epilepsy Phenome/Genome, P., Allen, A.S., Berkovic, S.F., Cossette, P., Delanty, N., Dlugos, D., Eichler, E.E., Epstein, M.P., Glauser, T. *et al.* (2013) De novo mutations in epileptic encephalopathies. *Nature*, **501**, 217–221.
33. Helbig, K.L., Farwell Hagman, K.D., Shinde, D.N., Mroske, C., Powis, Z., Li, S., Tang, S. and Helbig, I. (2016) Diagnostic exome sequencing provides a molecular diagnosis for a significant proportion of patients with epilepsy. *Genet. Med.*, doi:1038/gim.2015.186.
34. Stodberg, T., McTague, A., Ruiz, A.J., Hirata, H., Zhen, J., Long, P., Farabella, I., Meyer, E., Kawahara, A., Vassallo, G. *et al.* (2015) Mutations in SLC12A5 in epilepsy of infancy with migrating focal seizures. *Nat. Commun.*, **6**, 8038.
35. Palmieri, F. (2004) The mitochondrial transporter family (SLC25): physiological and pathological implications. *Pflugers Archiv.*, **447**, 689–709.
36. Inoue, K., Zhuang, L. and Ganapathy, V. (2002) Human Na+ -coupled citrate transporter: primary structure, genomic organization, and transport function. *Biochem. Biophys. Res. Commun.*, **299**, 465–471.
37. Koh, H.Y., Kim, D., Lee, J., Lee, S. and Shin, H.S. (2008) Deficits in social behavior and sensorimotor gating in mice lacking phospholipase Cbeta1. *Genes Brain Behav.*, **7**, 120–128.
38. Chang, N.S., Doherty, J. and Ensign, A. (2003) JNK1 physically interacts with WW domain-containing oxidoreductase (WOX1) and inhibits WOX1-mediated apoptosis. *J. Biol. Chem.*, **278**, 9195–9202.
39. Sumi, S., Marinaki, A.M., Arenas, M., Fairbanks, L., Shobowale-Bakre, M., Rees, D.C., Thein, S.L., Ansari, A., Sanderson, J., De Abreu, R.A. *et al.* (2002) Genetic basis of inosine triphosphate pyrophosphohydrolase deficiency. *Hum. Genet.*, **111**, 360–367.
40. Jilani, A., Ramotar, D., Slack, C., Ong, C., Yang, X.M., Scherer, S.W. and Lasko, D.D. (1999) Molecular cloning of the human gene, PNKP, encoding a polynucleotide kinase 3′-phosphatase and evidence for its role in repair of DNA strand breaks caused by oxidative damage. *J. Biol. Chem.*, **274**, 24176–24186.
41. Alazami, A.M., Hijazi, H., Kentab, A.Y. and Alkuraya, F.S. (2014) NECAP1 loss of function leads to a severe infantile epileptic encephalopathy. *J. Med. Genet.*, **51**, 224–228.
42. Campeau, P.M., Kasperaviciute, D., Lu, J.T., Burrage, L.C., Kim, C., Hori, M., Powell, B.R., Stewart, F., Felix, T.M., van den Ende, J. *et al.* (2014) The genetic basis of DOORS syndrome: an exome-sequencing study. *Lancet Neurol.*, **13**, 44–58.
43. Watabe-Uchida, M., John, K.A., Janas, J.A., Newey, S.E. and Van Aelst, L. (2006) The Rac activator DOCK7 regulates neuronal polarity through local phosphorylation of stathmin/Op18. *Neuron* **51**, 727–739.
44. Almeida, A.M., Murakami, Y., Layton, D.M., Hillmen, P., Sellick, G.S., Maeda, Y., Richards, S., Patterson, S., Kotsianidis, I., Mollica, L. *et al.* (2006) Hypomorphic promoter mutation in PIGM causes inherited glycosylphosphatidylinositol deficiency. *Nat. Med.*, **12**, 846–851.
45. Kato, M., Saitsu, H., Murakami, Y., Kikuchi, K., Watanabe, S., Iai, M., Miya, K., Matsuura, R., Takayama, R., Ohba, C. *et al.* (2014) PIGA mutations cause early-onset epileptic encephalopathies and distinctive features. *Neurology*, **82**, 1587–1596.
46. Martin, H.C., Kim, G.E., Pagnamenta, A.T., Murakami, Y., Carvill, G.L., Meyer, E., Copley, R.R., Rimmer, A., Barcia, G., Fleming, M.R. *et al.* (2014) Clinical whole-genome sequencing in severe early-onset epilepsy reveals new genes and improves molecular diagnosis. *Hum. Mol. Genet.*, **23**, 3200–3211.
47. Fores, O., Arro, M., Pahissa, A., Ferrero, S., Germann, M., Stukey, J., McDonough, V., Nickels, J.T., Jr., Campos, N. and Ferrer, A. (2006) Arabidopsis thaliana expresses two functional isoforms of Arvp, a protein involved in the regulation of cellular lipid homeostasis. *Biochim. Biophys. Acta*, **1761**, 725–735.
48. Garay, E., Campos, S.E., Gonzalez de la Cruz, J., Gaspar, A.P., Jinich, A. and Deluna, A. (2014) High-resolution profiling of stationary-phase survival reveals yeast longevity factors and their genetic interactions. *PLoS Genet.*, **10**, e1004168.
49. Palmer, E.E., Hayner, J., Sachdev, R., Cardamone, M., Kandula, T., Morris, P., Dias, K.R., Tao, J., Miller, D., Zhu, Y. *et al.* (2015) Asparagine Synthetase Deficiency causes reduced proliferation of cells under conditions of limited asparagine. *Mol. Genet. Metab.*, **116**, 178–186.
50. Reed, S.E., Staley, E.M., Mayginnes, J.P., Pintel, D.J. and Tullis, G.E. (2006) Transfection of mammalian cells using linear polyethylenimine is a simple and effective means of producing recombinant adeno-associated virus vectors. *J. Virol. Methods*, **138**, 85–98.

51. Livak, K.J. and Schmittgen, T.D. (2001) Analysis of relative gene expression data using real-time quantitative PCR and the 2(-Delta Delta C(T)) Method. *Methods*, **25**, 402–408.
52. Barch, M.J. and Association of Cytogenetic Technologists. (1991) *The ACT Cytogenetics Laboratory Manual*. Raven Press, New York.
53. Gietz, R.D., Schiestl, R.H., Willems, A.R. and Woods, R.A. (1995) Studies on the transformation of intact yeast cells by the LiAc/SS-DNA/PEG procedure. *Yeast*, **11**, 355–360.
54. Lee, C.S., Dagnino-Acosta, A., Yarotskyy, V., Hanna, A., Lyfenko, A., Knoblauch, M., Georgiou, D.K., Poche, R.A., Swank, M.W., Long, C. *et al.* (2015) Ca(2+) permeation and/or binding to CaV1.1 fine-tunes skeletal muscle Ca(2+) signaling to sustain muscle function. *Skelet. Muscle*, **5**, 4.
55. Dubois, N.C., Hofmann, D., Kaloulis, K., Bishop, J.M. and Trumpp, A. (2006) Nestin-Cre transgenic mouse line Nes-Cre1 mediates highly efficient Cre/loxP mediated recombination in the nervous system, kidney, and somite-derived tissues. *Genesis*, **44**, 355–360.